

# Flows developing around a finite rotating disk enclosed by a cylindrical casing

**Takashi Watanabe\* and Soma Endo**

Graduate School of Informatics, Nagoya University, Nagoya, 464-8601, Japan

\* Corresponding Author: watanabe@i.nagoya-u.ac.jp

**Abstract.** Numerical investigation has been performed on the flows around a rotating disk in a cylindrical casing. The sizes of the disk and the casing are finite, and the flow field has a radial clearance and an axial clearance. Taylor-Couette type flow develops in the radial clearance while the rotor-stator cavity flow appears in the axial clearance, and the interaction of the flows in these clearances makes complex flow developments. The flow structures are classified into some types including normal and anomalous modes in the radial clearance and circular and polygonal vortices in the axial clearance. The effect of the acceleration rate of the disk is estimated and it is found that the gradual increase of the disk angular velocity tends to form circular vortices in the normal mode.

## 1. Introduction

For the flow around a rotating disk, the three-dimensional shear layer with a cross flow has been studied [1-3]. In the present study, the flow around a finite rotating disk in a finite stationary cylindrical casing is numerically investigated. The flow field has a radial clearance between the disk rim and the side wall of the casing and an axial clearance between the surface of the disk and the end wall of the casing, and it can be regarded as a simple model of fluid machineries. One interest is the interaction of the flows in the clearances and it is expected that some flow structures appear.

The flow in the cylindrical cavity where the rotating and stationary coaxial disks are confined by a stationary cylindrical side wall has been studied in the experimental and numerical approaches. Schouveiler et al. [4, 5] used the visualization method and the ultrasonic Doppler velocimeter and experimentally showed that circular vortices and spiral vortices appeared in the case of wider axial clearance and turbulent spots and solitary waves emerged in the narrower axial clearance. They also offered their comment that the radial clearance of their experimental apparatus had some effects on the entire flows [5]. Poncet et al. [6] pointed out that the wave number of the spiral vortices was sensitive to the experimental condition. The annular cavity flow is the flow in the cylindrical cavity with a central axial hub. In this flow, the stationary hub suppressed the disturbances which grew in the Bödewadt layer on the stationary disk and propagated to the Ekman layer on the rotating disk [7]. On the other hand, the hub rotating with the disk enhanced the disturbances and made the flow turbulent [8-10]. Some reviews of the rotor-stator cavity flow with or without the hub have been reported [11, 12]. The flow around two or more disks connected by the hub can be found in the electric devices and chemical reactors. Hendriks [13] numerically predicted the flow in the hard disk drive with two platters and found that Taylor vortices appeared between the disk rim and the shroud of the casing. Washizu et al. [14] showed that the rib mounted on the shroud suppressed the pressure-based vibration of the hard disk drive. Meeuwse et al. [15] and de Beer et al. [16] examined the characteristics of the multi-phase and single-phase flow



in the multi-stage reactor, respectively, and Huang et al. [17] and Uenishi et al. [18] classified the polygonal flow structures found in the flow between two co-rotating disks shrouded by a cylindrical wall.

When the disk rotating in the casing has a finite thickness, centrifugal-force driven vortices emerge between the disk rim and the side wall of the casing [13]. Original Taylor vortices between the coaxial rotating cylinders have been studied in many areas [19-21]. When the cylinders have finite lengths and the stationary walls on their ends, the Ekman pumping mechanism forms the secondary flows on the end walls at the Reynolds number lower than that for the onset of Taylor vortices and the bifurcation phenomena become subcritical [22, 23]. With this shift of the physical situations, Taylor vortex flows show various structures including circular, wavy and modulated flows in normal and anomalous modes and the change of the incremental rate of the cylinders' angular velocities may bring multiple flow structures even though the Reynolds number and the geometrical configurations are fixed [24-26]. Recently, the stability of the quasi-Keplerian flow, in which the angular velocity radially decreases and the angular momentum radially increases, has been attracted researchers' interests [27-29], and some conclusions might be given [30].

We have carried out experimental and numerical investigations of the flow around a finite rotating disk in a cylindrical casing. In [31, 32], the numerical method was established and some experiments were performed. The numerical result showed good agreements with the experimental result of the circular vortices, spiral vortices and the phase velocity of the vortex structures. In [33], the effect of the width of the radial clearance on the flow was estimated. In the present study, the effect of the axial clearance width is numerically considered. The flows in the radial and axial clearances are classified and the diagrams of the flow structures in the space of the Reynolds number and the axial clearance width are presented. Two acceleration rates of the disk are used and their effect on the final flow structures is shown.

## 2. Formulation

The schematic construction of the flow field is represented in figure 1. The cylindrical casing is stationary and its inner radius and the length are  $r_c$  and  $h_c$ , respectively. The rotating disk with a driving shaft is set at the center of the casing. The radius and the thickness of the disk are  $r_d$  and  $h_d$ , respectively, and the radius of the driving shaft is  $r_s$ . The disk rotates with the driving shaft at the angular velocity  $\omega$ . The coordinate system is the cylindrical system  $(r, \theta, z)$ . Its origin is at the center of the lower end wall of the casing and the  $z$  axis aligns with the central axis of the flow field. In numerical method, the governing equations are made nondimensional by the reference length of the disk radius, the reference circumferential velocity at the disk rim and the reference time given by the reciprocal of the angular velocity. The size of the casing is fixed and  $r_c = 1.118$  and  $h_c = 0.3150$ . The shaft radius  $r_s$  is 0.0787 and it is small enough not to have any influence on the flow field [6]. Eight disks with  $h_d$  from 0.1575 to 0.2677 are introduced to see the effect of the axial clearance width. The thickness ratios  $\gamma$  defined by the fraction  $h_d / h_c$  are 0.50, 0.55, 0.60, 0.65, 0.70, 0.75, 0.80 and 0.85.

In order to estimate the dimensional phenomena from the nondimensional results, the dimensional disk radius  $D$  of 127 [mm], the dimensional angular velocity  $\Omega$  [1/s] and the kinematic viscosity  $\nu$  of 4.0 [mm<sup>2</sup>/s] of glycerin aqueous solution are assumed. The Reynolds number  $Re$  is given by  $D^2 \Omega / \nu$  and the dimensional time is estimated from the nondimensional time  $t$  by  $4032 \times t / Re$ .

The governing equations are the equation of continuity and the unsteady three-dimensional incompressible Navier-Stokes equations:

$$\nabla \cdot \mathbf{u} = 0, \quad (1)$$

$$\frac{\partial \mathbf{u}}{\partial t} + \nabla(\mathbf{u}\mathbf{u}^T) = -\nabla p + \frac{1}{Re} \nabla^2 \mathbf{u}, \quad (2)$$

where  $\mathbf{u}$  is the velocity vector with its radial, circumferential and axial components  $u$ ,  $v$  and  $w$ , and  $p$  is the pressure. The boundary condition is the no-slip condition on the solid walls. Initially, the flow is at rest in the entire region. The discretization method is based on the finite difference method [34] and the

whole circumferential region of  $\theta$  from 0 to  $2\pi$  is adopted. In the case that the acceleration time of the disk is zero, the disk is rotated suddenly at the angular velocity giving a prescribed Reynolds number. When the acceleration time is finite, the angular velocity is linearly increased. The acceleration rate  $\alpha$  is defined by the incremental of the Reynolds number in one dimensional second.

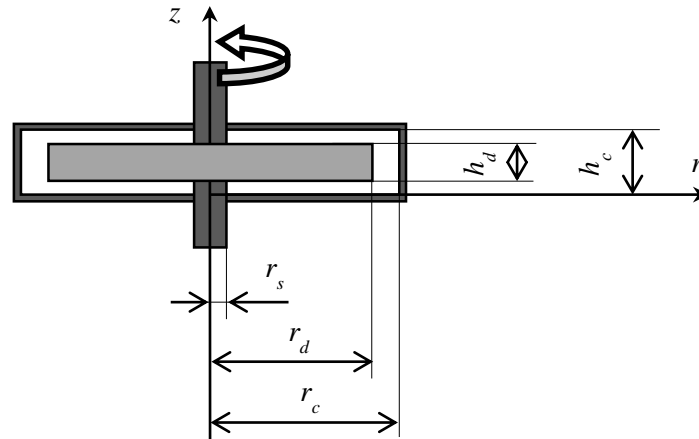


**Figure 1.** Schematic drawing of the flow field.

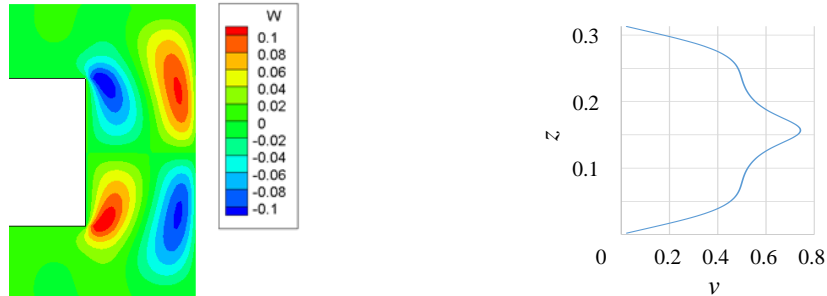
### 3. Results and Discussion

#### 3.1. Flow structures in the radial clearance

The modes of Taylor vortex flows between rotating cylinders with finite lengths have been determined by the number of vortices in the meridional section and the flow direction on the stationary end wall [35]. In the flows around a rotating disk in a cylindrical casing, flow modes similar to those of Taylor vortex flows can be found in the radial clearance between the disk rim and the side wall of the casing. In the present study, the flow structures are classified in four modes. Figure 2 shows the flow in the normal 2-cell mode. The thickness ratio  $\gamma$  is 0.5, the Reynolds number  $Re$  is 3,000 and the acceleration rate  $\alpha$  is 200. Figure 2 (a) depicts the contour of the axial velocity component  $w$  in the meridional section ( $r$ - $z$  plane) near the radial clearance, and the disk rim is on the left side and the side wall of the casing is on the right side. In the upper half of the figure, a pair of a cold color region on the left and a warm color region on the right represents a toroidal vortex rotating in the counterclockwise direction. The lower half denotes the vortex rotating in the clockwise direction. These two vortices have radially inward flows on the upper and lower end walls of the casing. The mode of Taylor vortex with a radially inward flow on the end wall is normal [35]. The flow in figure 2 (a) has two vortices (two cells) in the normal mode and the flow mode is the normal 2-cell mode. The flow between two vortices is radially outward near the midplane in the axial direction. Figure 2 (b) shows the profile of the circumferential velocity component  $v$  (abscissa) along the axial direction (ordinate) at midsection of the radial clearance ( $r = 1.06$ ). The cusp at the axial midplane results from the convection of the circumferentially accelerated flow near the rotating disk rim by the radially outward flow.

Figure 3 shows the normal 4-cell mode in the radial clearance. In figure 3 (a), four pairs of the warm and cold regions, from upper to lower, indicate the vortices rotating in the counterclockwise, clockwise, counterclockwise and clockwise directions, respectively. The flows of the vortices on the end walls are radially inward and they are normal. The flow has three boundaries between the four vortices. The flows near the upper-most and the lower-most boundaries are radially outward and the flow near the mid-boundary is inward. The radially outward and inward flows carry accelerated and decelerated

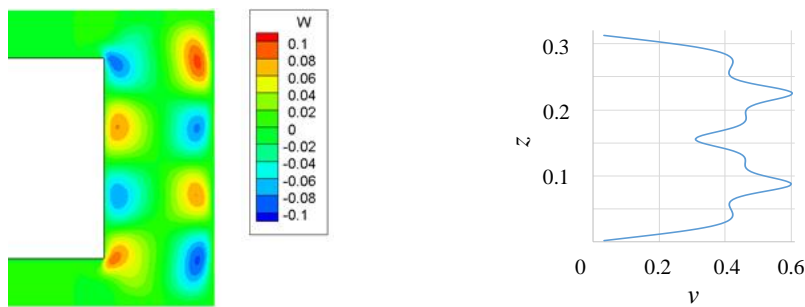
circumferential flows, respectively, and the profile of the circumferential velocity component has two maxima and one minimum as shown in figure 3 (b).



(a) Contour of the axial velocity component near the radial clearance.

(b) Profile of the circumferential velocity component at  $r = 1.06$ .

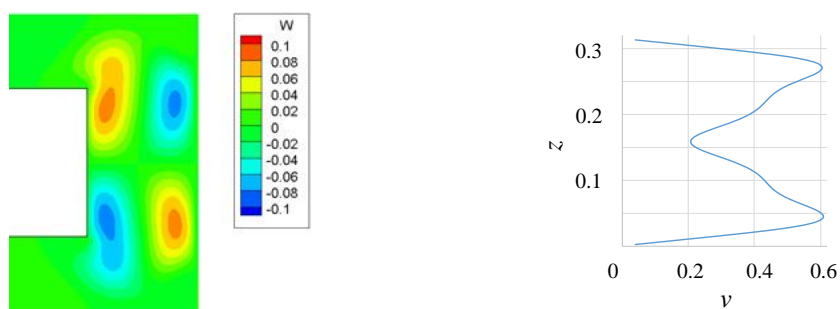
**Figure 2.** Normal 2-cell mode.  $\gamma = 0.5$ ,  $Re = 3000$ ,  $\alpha = 200$ .



(a) Contour of the axial velocity component near the radial clearance.

(b) Profile of the circumferential velocity component at  $r = 1.06$ .

**Figure 3.** Normal 4-cell mode.  $\gamma = 0.7$ ,  $Re = 5000$ ,  $\alpha = 1000$ .



(a) Contour of the axial velocity component near the radial clearance.

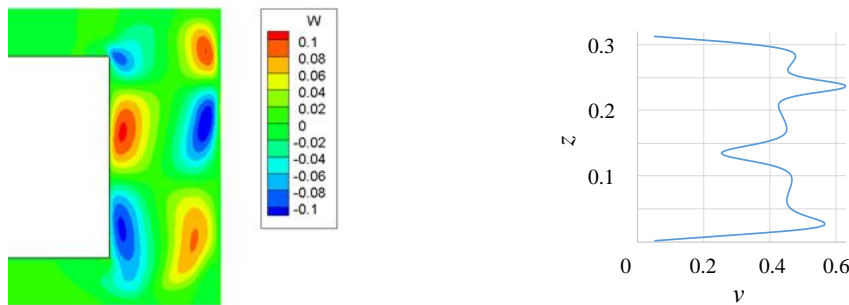
(b) Profile of the circumferential velocity component at  $r = 1.06$ .

**Figure 4.** Anomalous 2-cell mode.  $\gamma = 0.5$ ,  $Re = 3000$ ,  $\alpha = 1000$ .

The flow in figure 4 has two vortices in the radial clearance. The upper one and the lower one in figure 4 (a) rotate in the clockwise and counterclockwise directions, respectively. This means that the flows on the end walls are radially outward and the mode of the vortices is anomalous [35]. The flow mode is the anomalous 2-cell mode. The radial flow near the axial midplane is inward and the profile of

the circumferential velocity component in figure 4 (b) has a minimum at the midplane, while it has peaks near the end walls.

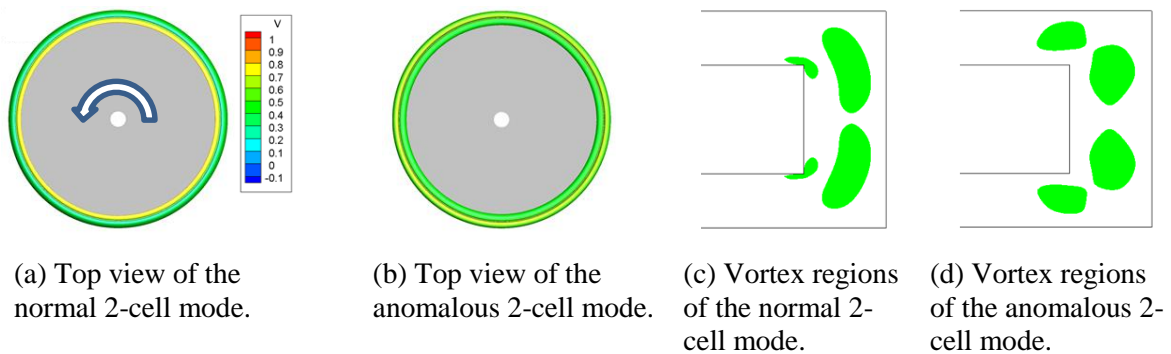
Figure 5 shows an asymmetric flow pattern with three vortices. In figure 5 (a), the lowest vortex rotates in the counterclockwise direction and it has a radially outward flow on the lower end wall. The lowest vortex is anomalous, and the flow mode is the anomalous 3-cell mode. The three vortices have two boundaries and the profile in figure 5 (b) has its maximum and minimum near these boundaries.



(a) Contour of the axial velocity component near the radial clearance.

(b) Profile of the circumferential velocity component at  $r = 1.06$ .

**Figure 5.** Anomalous 3-cell mode.  $\gamma = 0.7$ ,  $Re = 7000$ ,  $\alpha = 500$ .



(a) Top view of the normal 2-cell mode.

(b) Top view of the anomalous 2-cell mode.

(c) Vortex regions of the normal 2-cell mode.

(d) Vortex regions of the anomalous 2-cell mode.

**Figure 6.** Steady state with circular vortices in the normal and anomalous 2-cell modes.

(a) and (c):  $\gamma = 0.5$ ,  $Re = 3000$ ,  $\alpha = 1000$ . (b) and (d):  $\gamma = 0.5$ ,  $Re = 3000$ ,  $\alpha = 200$ .

(a) and (b): Contours of  $Q = 1.0$ . (c) and (d): Vortex regions at  $0.0 \leq Q \leq 1.0$ .

### 3.2. Flow structures in the axial clearance

In this subsection, the three-dimensional flow structures in the axial clearance are visualized by the second invariant of the velocity gradient tensor ( $Q$  value) formulated in the cylindrical coordinate system [36]. Figure 6 represents the flow structures as the contours of  $Q = 1.0$ , which are in the steady state and in the normal 2-cell mode. The rotating direction of the disk is counterclockwise. The thickness ratio  $\gamma$  is 0.5 and the Reynolds number  $Re$  is 3,000. Figures 6 (a) and (b) show the normal mode flow at  $\alpha = 1,000$  and the anomalous mode flow at  $\alpha = 200$ , respectively. The color on the contours corresponds to the value of the circumferential velocity component  $v$  shown in the legend. The vortex structures are confined in the radial clearance and they are axisymmetric and circular. Figures 6 (c) and (d) depict the vortex regions indicated by the value of  $Q$  from 0.0 to 1.0 in the meridional sections near the radial clearance of the flows in figures 6 (a) and (b), respectively. The flow in the normal mode in figure 6 (c) has small vortex regions at the edges of the disk, and these small structures correspond to the inner yellow ring with higher circumferential velocity component in figure 6 (a). In figure 6 (d) of the anomalous mode flow, vortex regions appear above and below the disk and two vortex regions emerge

in the radial clearance. The latter two regions have higher circumferential velocity component near the end walls and they can be seen in the outer yellow region in figure 6 (b).

Figure 7 shows the flow which appears at the moderate Reynolds number and has polygonal vortices. The mode is the anomalous 2-cell mode. Figures 7 (a) and (b) represent the contours of  $Q = 1.0$  and the legend of the color map is the same as that in figure 6. The vortex structure in figure 7 (a) is a nonagon with nine almost periodic patterns and the circumferential wave number is 9. Figure 7 (b) is the bird's eye view. Intermittent and elongated patterns emerge at the top and the bottom of the figure. The two vortices in the radial clearance are in the wavy state. In order to see the details of the flow pattern, the vortex regions at  $Q$  from 0.0 to 1.0 in the meridional sections denoted by the numbers from (1) to (5) in figure 7 (b) are shown in figure 7 (c). Other than the four main vortex regions similar to those in figure 6 (d), small vortex regions appear and/or disappear at the upper-right and lower-right corners of the casing. These small vortices attached to the anomalous vortices were called extra vortices by Nakamura et al. [24] who investigated Taylor vortex flows in very short cylinders. The circumferential variation of the size and the shape of the extra vortex makes the polygonal vortex in the axial clearance. Figure 8 describes the flow in the anomalous 2-cell mode, which has more frequent periodicity and bead-like patterns. The wave number is 30 and the coherent structures appear at the corners of the casing.

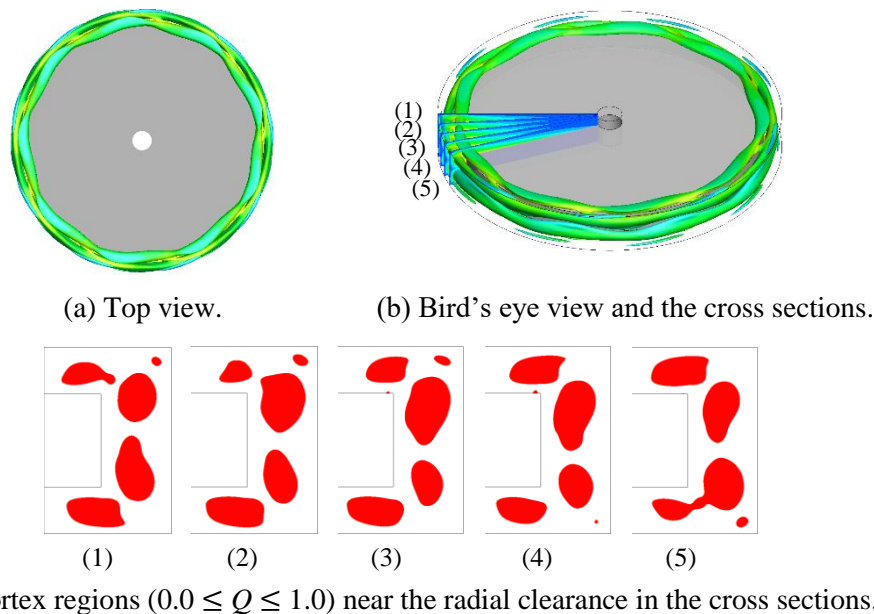


**Figure 7.** Wavy state with polygonal vortices in the anomalous 2-cell mode and the wave number of 9.  $\gamma = 0.5$ ,  $Re = 4000$ ,  $\alpha = 200$  and  $Q = 1.0$ .

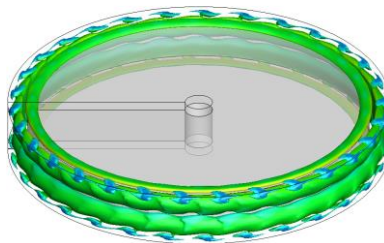
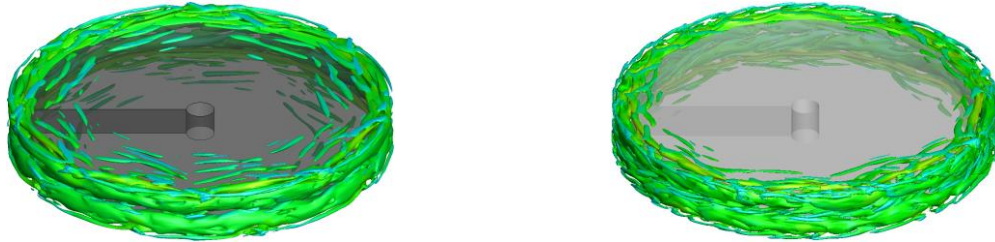


**Figure 8.** Wavy state with polygonal vortices in the anomalous 2-cell mode and the wave number of 30 (bead-like pattern).  $\gamma = 0.7$ ,  $Re = 8000$ ,  $\alpha = 1000$  and  $Q = 1.0$ .



The flow structures at higher Reynolds number are shown in figure 9, where the flow mode is the anomalous 2-cell mode. In the flow in figure 9 (a) at  $\gamma = 0.50$ , the disturbances generated in the radial clearance propagate onto the inner region of the disk and form spiral vortices with some periodicities. Figure 9 (b) is the flow at  $\gamma = 0.65$ . Only a few spiral vortices are found in the axial clearance and the flow structure is unconstructed. Though the state of the flows in the radial clearances in figures 9 (a) and (b) is a turbulent state, the flows show some coherence similar to that which has been called herring-bone-like streaks [37].



(a) Spiral vortices in the axial clearance.  $\gamma = 0.50$ . (b) Unconstructed flow structure.  $\gamma = 0.65$ .

**Figure 9.** Turbulent state.  $Re = 20,000$ ,  $\alpha = 10,000$  and  $Q = 1.0$ .

**Table 1.** Final flow structures <sup>a</sup>.

(a) Sudden acceleration.

	$\gamma$							
	0.50	0.55	0.60	0.65	0.70	0.75	0.80	0.85
3000	C	C	C	C	C	C	C	C
4000	P	C	C	C	C	C	C	C
5000	P	P	C	C	C	C	C	C
6000	P	P	C	C	C	C,S	C	C
7000	P	P	S	C	C	C,S	C	C
8000	P	P	S	S	S	S	C	C
9000	P	P	S	S	S	S	C	C
10000	P	P	P	S	S	S	C	C
11000	P	P	P	S	S	S	C	C
12000	P	P	P	S	S	S	C	C
13000	P	P	P	S	S	S	C	C
14000	P	P	P	S	S	S	C	C
15000	P	P	P	S	S	S	C,S	C
16000	P	P	P	S	S	S	C,S	C
17000	P	P	P	S	S	S	S	C
18000	P	P	P	S	S	S	S	C
19000	P	P	P	S	S	S	S	C
20000	P	P	P	S	S	S	S	C

(b) Gradual acceleration at  $\alpha = 1,000$ .

	$\gamma$							
	0.50	0.55	0.60	0.65	0.70	0.75	0.80	0.85
3000	C	C	C	C	C	C	C	C
4000	P	C	C	C	C	C	C	C
5000	P	P	C	C	C	C	C	C
6000	P	P	C	C	C	C	C	C
7000	P	P	S	C	C,S	C	C	C
8000	P	P	S	S	S	C	C	C
9000	P	P	S	S	S	C	C	C
10000	P	P	S	S	S	C,S	C	C
11000	P	P	P	S	S	C,S	C	C
12000	P	P	P	S	S	S	C	C
13000	P	P	P	S	S	S	C	C
14000	P	P	P	S	S	S	C	C
15000	P	P	P	S	S	S	C	C
16000	P	P	P	S	S	S	C	C
17000	P	P	P	U	S	S	C	C
18000	P	P	P	U	S	S	C,S	C
19000	P	P	P	U	S	S	C,S	C
20000	P	P	P	U	S	S	C,S	C

<sup>a</sup> yellow: normal 2-cell mode, orange: normal 4-cell mode, green: anomalous 2-cell mode, blue: anomalous 3-cell mode. C: circular vortices, P: polygonal vortices, S: spiral vortices, U: unconstructed flow.

### 3.3. Effect of the acceleration rate on the flow structures

The final flow structures with the sudden acceleration and the gradual acceleration of  $\alpha = 1,000$  are presented in tables 1 (a) and (b). In each table, the rows are the Reynolds number  $Re$  and the columns are the thickness ratio  $\gamma$ . The colors distinguish the flow structures in the radial clearance, which are the normal 2-cell mode (yellow), the normal 4-cell mode (orange), the anomalous 2-cell mode (green) and the anomalous 3-cell mode (blue). The characters denote the axial clearance flow structures with the circular vortices (C), polygonal vortices (P), spiral vortices (S) and unconstructed flow (U). In the condition of the sudden acceleration in table 1 (a), when the thickness ratio is 0.85 and the axial clearance is the narrowest, the flow mode in the radial clearance is the normal 2-cell mode and the circular vortices appear in the axial clearance at the Reynolds numbers up to 20,000. At  $\gamma = 0.80$ , the anomalous 2-cell mode and spiral vortices are found at the higher Reynolds numbers. The flow in the anomalous 3-cell mode appears at  $Re = 15,000$  and 16,000 and this flow has the circular vortices near the end wall where the normal vortex appears and the spiral vortices near the end wall on which the anomalous vortex emerges. At smaller thickness ratios, the range of the Reynolds number at which the normal 2-cell mode emerges is limited. At  $\gamma \leq 0.55$ , the anomalous 2-cell mode occurs in the entire Reynolds number range investigated in the present study. At the thickness ratio not less than 0.65, the flow tends to have spiral vortices. When the thickness ratio is not more than 0.60, the polygonal vortices are dominant. Table 1 (b) in the case of the gradual acceleration shows that the normal 4-cell mode with circular vortices tends to appear more often at the moderate thickness ratios, while the anomalous mode seems to occur at the higher Reynolds numbers. At  $\gamma = 0.65$  and the higher Reynolds numbers, the flow has no clear spiral vortices and it is unconstructed. The range of the Reynolds number at which the flow in the anomalous 2-cell mode has the polygonal or spiral vortices is almost fixed in the flows with the sudden and gradual rotations at  $\gamma \leq 0.65$ . Regardless of the acceleration conditions of the disk, the normal mode flows have circular vortices.

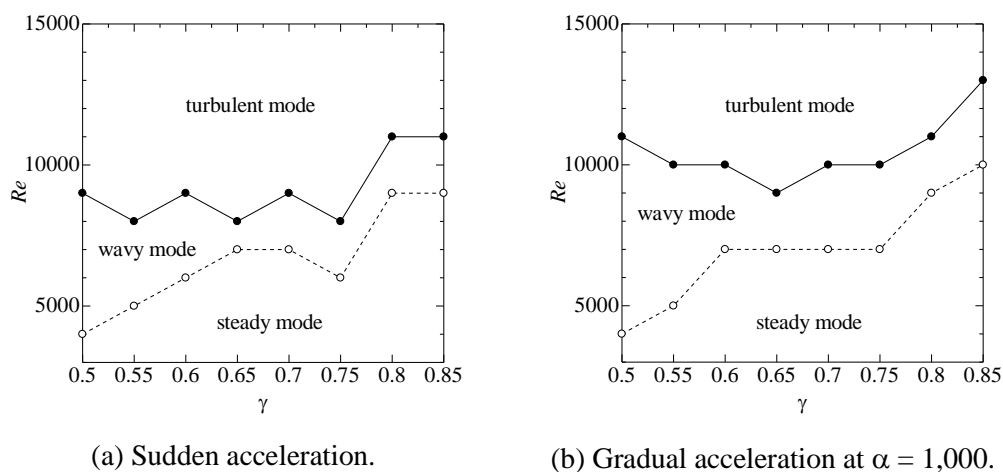


**Figure 10.** Flow state diagram.

The diagrams for the onset of the steady, wavy and turbulent states mentioned in subsection 3.2 are shown in figure 10. The abscissa is the thickness ratio and the ordinate is the Reynolds number. The open circles and the filled circles denote the lower limits of the appearances of the wavy state and the turbulent state, respectively. The sudden start case is in figure 10 (a) and the gradual start case at  $\alpha = 1,000$  is in figure 10 (b). In both acceleration cases, the critical Reynolds number for the wavy state tends to increase as the thickness ratio becomes larger and the axial clearance turns narrower, and the effect of the acceleration rate on the critical values is not large. The diagram at the sudden acceleration shows the minima of the critical values at  $\gamma = 0.75$ . When  $\gamma$  is 0.75, the fraction of the radial clearance



width to the thickness of the disk is 2.0 and the fraction of the axial clearance width to the width of the radial clearance is 0.333. This geometrical condition may contribute to make the minima and it is expected that this can be clarified by the investigation of the scenario of the flow development from the stationary state. The Reynolds number for the onset of the turbulent state is almost constant at  $\gamma \leq 0.75$ , and it increases at  $0.80 \leq \gamma$ . This means that the narrower axial clearance suppresses the growth of the disturbances. The critical value of the turbulent state in the case of the gradual acceleration is about 100 larger than the value at the sudden acceleration.

#### 4. Conclusion

The flow around a rotating disk in a cylindrical casing is numerically investigated. The Reynolds number based on the disk radius and the circumferential velocity at the disk rim is from 3,000 to 20,000. Eight disks are considered and the ratio of the disk thickness to the length of the casing is from 0.50 to 0.85. The sudden acceleration and the gradual acceleration of the disk rotation are adopted. By following the categorization of Taylor vortex flows, the flow structures in the radial clearance are classified into the normal and anomalous modes with 2, 3 and 4 cells. The flows in the axial clearance show the circular vortices, polygonal vortices with various wave numbers, spiral vortices and the unconstructed flow. When the disk is thick and the axial clearance is narrow, the normal mode easily appears in the radial clearance and the flow has circular vortices. As the thickness of the disk becomes thinner, the range of the Reynolds number at which the anomalous mode appears widens at the higher Reynolds numbers. The flow includes the spiral vortices at the moderate thickness ratios. At lower thickness ratios, the flow in the anomalous mode has the polygonal vortices resulted from the circumferential shape change of the extra vortices associated with the anomalous vortices. When the acceleration of the disk is gradual, the normal mode likely emerges and the critical Reynolds number between the wavy state and the turbulent state increases. The Hopf bifurcation from the steady state to the wavy state is not largely affected by the acceleration rate.

#### Acknowledgement

This work is partly supported by the JSPS Grants-in-Aid for Scientific Research 15K05791.

#### References

- [1] Jasmine H A and Gajjar T S B 2005 *Phil. Trans. R. Soc. A* **363** pp 1131-44
- [2] van Eeten K M P, van der Schaaf J, Schouten J C and van Heijst G J F 2012 *Phys. Fluids* **24** 033601
- [3] Lingwood R J and Alfredsson P H 2015 *Trans. ASME App. Mech. Rev.* **67** 030803
- [4] Schouveiler L, Le Gal P and Chauve M P 1998 *Phys. Fluids* **10** pp 2695-7
- [5] Schouveiler L, Le Gal P and Chauve M P 2001 *J. Fluid Mech.* **443** pp 329-50
- [6] Poncet S, Serre É and Le Gal P 2009 *Phys. Fluids* **21** 064106
- [7] Serre E, Crespo del Arco E and Bontoux P 2001 *J. Fluid Mech.* **434** pp 65-100
- [8] Séverac É Poncet S, Serre É and Chauve M-P 2007 *Phys. Fluids* **19** 085113
- [9] Viazzi S, Poncet S, Serre E, Randriamampianina A and Bontoux P 2012 *Flow Turbulence Combust.* **88** pp 63-75
- [10] Makino S, Inagaki M and Nakagawa M 2015 *Flow Turbulence Combust.* **95** pp 399-413
- [11] Saric W S, Reed H L and White E B 2003 *Annu. Rev. Fluid Mech.* **35** pp 413-40
- [12] Launder B, Poncet S and Serre E 2010 *Annu. Rev. Fluid Mech.* **42** pp 229-48
- [13] Hendriks F 2010 *Microsyst. Technol.* **16** pp 93-101
- [14] Washizu T, Lubisch F and Obi S 2013 *Flow Turbulence Combust.* **91** pp 607-21
- [15] Meeuwse M, van der Schaaf J and Schouten J C 2012 *AIChE J.* **56** pp 247-55
- [16] de Beer M M, Keurentjes J T F Schouten J C and van der Schaaf J 2014 *Chem. Engng. J.* **242** pp 53-61
- [17] Huang R F and Hsieh M K 2011 *Exp. Fluids* **51** pp 1529-47
- [18] Uenishi R, Tsugawa S, Maeda T, Uesaka M, Watanabe T, Tanigawa H and Hirata K 2016 *Proc. the 7th TSME Int. Conf. on Mech. Engng. (Chiang Mai)* TSF0025
- [19] Tagg R 1994 *Nonlinear Science Today* **4** pp 1-24
- [20] Fardin M A, Perge C and Taberlet N 2014 *Soft Matter* **10** pp 3523-35
- [21] Grossmann S, Lohse D and Sun C 2016 *Annu. Rev. Fluid Mech.* **48** pp 53-80

- [22] Benjamin T B 1978 *Proc. Royal Soc. Lnd. A* **359** pp 1-26
- [23] Benjamin T B 1978 *Proc. Royal Soc. Lnd. A* **359** pp 27-43
- [24] Nakamura I and Toya Y 1996 *Acta Mechanica* **117** pp 33-46
- [25] Watanabe T, Furukawa H and Nakamura I 2002 *Phys. Fluids* **14** pp 333-41
- [26] Furukawa H, Watanabe T, Toya Y and Nakamura I 2002 *Phys. Rev. E* **65** 036306
- [27] Ji H, Burin M, Schartman E and Goodman J 2006 *nature* **444** 343-6
- [28] Avila 2012 *Phys. Rev. Lett.* **108** 124501
- [29] Edlund E M and Ji H 2015 *Phys. Rev. E* **92** 043005
- [30] Lopez J M and Avil M 2017 *J. Fluid Mech.* **817** pp 21-34
- [31] Watanabe T and Furukawa H 2010 *Exp. Fluids* **48** pp 631-6
- [32] Watanabe T and Furukawa H 2010 *Phys. Fluids* **22** 114107
- [33] Hara S, Watanabe T, Furukawa H and Endo S 2015 *J. Visualization* **18** pp 501-10
- [34] Lygren M and Andresson H I 2001 *J. Fluid Mech.* **426** pp 297-326
- [35] Nakamura I, Toya Y, Yamashita S and Ueki Y 1990 *JSME Int. J. Ser. II* **33** pp 685-91
- [36] Jeong J and Hussain F 1995 *J. Fluid Mech.* **285** pp 69-94
- [37] Dong S 2007 *J. Fluid Mech.* **587** pp 373-93